

# Layers of semiflexible chain molecules endgrafted at interfaces: An off-lattice Monte Carlo simulation

F. M. Haas

*Institut für Physik, Universität Mainz, D-55099 Mainz, Germany*

R. Hilfer

*Institut für Physik, Universität Mainz, D-55099 Mainz, Germany  
and International School for Advanced Studies, Via Beirut 2-4, 34013 Trieste, Italy*

K. Binder

*Institut für Physik, Universität Mainz, D-55099 Mainz, Germany*

(Received 11 July 1994; accepted 8 November 1994)

A coarse-grained model for surfactant chain molecules at interfaces in the high density regime is studied using an off-lattice Monte Carlo technique. The surfactant molecules are modeled as chains consisting of a small number (e.g., seven) of effective monomers. For the modeling of lipid monolayers, each effective monomer is thought to represent several  $\text{CH}_2$  groups of the alkane chain, but applications of the model to other polymers end grafted at solid surfaces also should be possible. The head segments are restricted to move in the adsorption plane, but otherwise do not differ from the effective monomers, which all interact with Lennard-Jones potentials. Bond angle and bond length potentials take into account chain connectivity and chain stiffness. The advantage of this crude model is that its phase diagram can be studied in detail. Temperature scans show two phase transitions, a tilting transition at low temperatures between a tilted and an untilted phase, and a melting transition at high temperatures where the lattice of head groups loses its crystalline order. © 1995 American Institute of Physics.

## I. INTRODUCTION

Langmuir monolayers have recently attracted much attention because of their connection to Langmuir-Blodgett films which may be of interest for device applications. A very rich phase diagram is observed experimentally.<sup>1</sup> Many phase transitions in Langmuir films can be seen in direct comparison to the transitions observed in liquid crystals.<sup>2</sup> Nevertheless the temperature behavior of these systems is not yet well understood, because the surfactant molecules possess many degrees of freedom and the various phases involve both inter- and intramolecular degrees of freedom.

It is a challenging problem to identify the nature of the observed phase transitions experimentally,<sup>3,4</sup> especially in the liquid-condensed regime, because many of them occur in a small temperature range. The same general form of the phase diagram is observed experimentally for a large variety of film molecules.<sup>3</sup> The microscopic interactions are not always well understood, and consequently various types of models with different degrees of simplification have been developed.<sup>5-20</sup> The relevance of microscopic chemical detail or the macroscopic phase behavior of lipid monolayers remains an active research topic<sup>5-7,14-17,20</sup> but will remain outside of consideration here. Apart from monolayers of fatty acids or phospholipids at the air-water interface, there are many other examples where more or less stiff polymers are grafted at surfaces of fluids and solids.<sup>21-25</sup> Also in systems of other such surfactants sometimes interesting phase transitions have been observed.

The present article hence does not aim at trying to explain the specific properties of a particular material, but

rather tries to develop a coarse-grained model that exhibits some of the general features of the observed phase behavior, but is still simple enough for extensive computer simulation over wide ranges of temperature and densities. In coarse-grained models only those degrees of freedom of a full microscopic description are kept which are believed to be most essential for the observed phenomena. These models require less computational effort than fully microscopic calculations, thus allowing one to simulate a larger number of surfactant molecules. This is particularly important for the study of phase transitions. Many authors used lattice models as a coarse-grained description,<sup>8-10</sup> but this oversimplification prevented a description of all phase transitions at high surface densities and the results were sometimes affected by lattice artifacts (e.g., cubic lattices allow only a square rather than the correct triangular structure of the head group lattice<sup>10</sup>). In previous works<sup>11,12</sup> we focused on the transition from a phase with uniformly tilted molecules to one in which the molecules were untilted. The rigid rod model used in those articles neglects all intramolecular degrees of freedom by coarse graining the alkane chains into perfectly rigid rods. The rods can rotate freely in continuous space around anchoring points forming a rigid hexagonal lattice.

In the present article we consider a coarse-grained continuum model of semiflexible chains. The molecules are represented by chains of a small number of effective monomers. Each monomer is thought to represent a group of about 2-5 successive chemical monomers (e.g.,  $\text{CH}_2$  or  $\text{CF}_2$  groups) of the chain molecule. This coarse-graining along the chain is essential, since we do not take into account any torsional

potentials. In previous work on single alkane chains<sup>26,27</sup> it was shown that the distribution of the lengths of effective segments formed in this way can be thought of as a result of an effective bond length potential for the coarse-grained model. Similarly, the distribution of the angle between subsequent effective bonds can also be modeled by a suitable effective potential for bond angles, and the correct persistence length of the chains can thus be reproduced, at least roughly. Thus effective intramolecular potentials are introduced to take into account chain connectivity and chain stiffness. We feel that an off-lattice model is advantageous especially at high surface densities. Although lattice models allow more monomer trial moves per unit time the relaxation times will be much larger than in a continuous model in view of the restricted freedoms of motion.

In Sec. II we now specify the model in detail and motivate the choice of its parameters. In Sec. III we analyze the classical ground state of our model, because we feel that understanding the nature and detailed structure of the ground state is essential information of the behavior at elevated temperatures. Section IV describes our simulation techniques, while Sec. V gives a detailed overview of our simulation results. Finally, Sec. VI gives a discussion and outlook on the further development of our model, which at this point is still too coarse grained to allow a quantitative comparison with real materials, but already gives useful qualitative insight.

## II. THE MODEL

Our model represents a film of rodlike amphiphilic molecules whose heads are attached to a surface (Fig. 1). The surface is ideally flat, structureless and rigid, and hence at this level of idealization we do not distinguish whether the substrate is a fluid or a solid. Each grafted molecule is a chain of seven effective monomers. If one accepts the above mapping to a chemically realistic alkane chain, this would correspond to a degree of polymerization of about 20. The monomers within a chain are connected by a harmonic potential with minimum at distance  $d_0$  and spring constant  $c_{bl} > 0$

$$V_{bl}(d) = \begin{cases} c_{bl}(d-d_0)^2: & \text{for } |d-d_0| \leq d_{bl} \\ \infty: & \text{for } |d-d_0| > d_{bl} \end{cases}, \quad (1)$$

which is cutoff at  $d_{bl} > 0$ . In addition to the harmonic bond length potential, which ensures the connectivity of the chain-like molecule, we introduce a bond angle potential to simulate chain stiffness. The bond angle potential is chosen as

$$V_{ba}(\theta_i) = c_{ba}[1 + \cos(\theta_i)], \quad (2)$$

where  $c_{ba} > 1$  is the force constant and  $\theta_i$  is the angle formed by the three monomers  $i-1, i, i+1$  ( $i=1, \dots, l-2$ ). Here we have numbered the  $l$  monomers, such that the head group has index 0. The head groups are restricted to move in the  $xy$  plane.

All monomers except nearest neighbors within a chain interact with a Lennard-Jones potential, which is truncated at  $d = d_{LJ}\sigma$  and shifted so that it is zero there

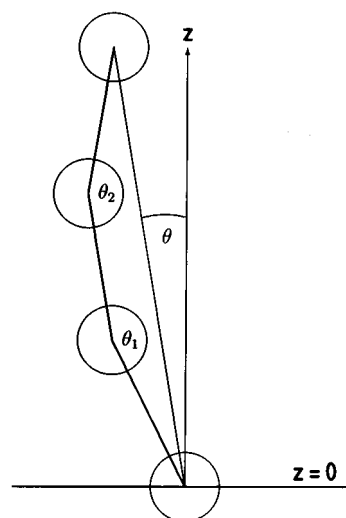


FIG. 1. Schematic description of the model studied in the present work: The lipid chain molecules are represented by chains of effective segments whose head groups are restricted to move in the adsorption plane at  $z=0$ . The bond vectors connecting neighboring chain segments form angles  $\theta_i$ . The tilt angle  $\theta$  of one molecule is defined as the angle between the surface normal  $\hat{z}$  and the end-to-end vector of the chain.

$$V_{LJ}(d) = \begin{cases} \epsilon[(\sigma/d)^{12} - 2(\sigma/d)^6] - \epsilon[(1/d_{LJ}^{12}) - 2(1/d_{LJ}^6)]: & \text{for } d \leq d_{LJ}\sigma \\ 0: & \text{for } d > d_{LJ}\sigma \end{cases}, \quad (3)$$

where  $\epsilon$  measures the strength and  $\sigma$  the range of this potential and  $d$  is the distance between two monomers.

Our rodlike chain molecules are a coarse-grained representation for amphiphilic molecules such as fatty acids or phospholipids. Such molecules are known to exist in a stretched conformation at low temperatures.<sup>3</sup> The restriction of the head groups to the  $xy$  plane represents a strong interaction of the polar heads with the water surface. Capillary waves and the molecular structure of the water surface are neglected in our model. Similarly all chemical detail of the lipid molecules, such as size and shape of the head groups and tails are averaged out in our coarse-grained description. Similar united atom models have been investigated using molecular dynamics simulations.<sup>13-17</sup> In these united atom models a Lennard-Jones force center represents a  $\text{CH}_3$  or  $\text{CH}_2$  group, and there is still a torsional potential present, while in our model several such groups are represented by a single Lennard-Jones center, and the torsional potential for these effective bonds is zero. As is well known, the approach to equilibrium for chain molecules without torsional potential is much faster, and therefore our crude model is better suited for the study of phase transitions than the more realistic models.<sup>13-17</sup> Previous continuum Monte Carlo (MC) simulations have studied the rigid rod model suggested by Safran *et al.*<sup>18</sup> where the polar head groups are fixed on one- and two-dimensional lattices.<sup>11,12</sup>

In our simulation we concentrate on chains of length  $l=7$ . We choose dimensionless units by setting  $\epsilon=1$  and  $\sigma=1$ . In these units the bond length  $d_0$  is set to  $d_0=0.7$ ,  $d_{bl}=0.2$ , and  $d_{LJ}=2$ . This choice ensures that the rods do not intersect each other for the temperature range of our simulations. The energy scales  $c_{bl}$  and  $c_{ba}$  of the intrachain potentials are chosen to be  $c_{bl}=100$  and  $c_{ba}=10$  which is large in comparison to the Lennard-Jones interchain potentials, i.e.,  $c_{bl}, c_{ba} \gg \epsilon$ . Our model description is completed by choosing a rectangular simulation area in the  $xy$  plane with sidelengths  $L_x$  and  $L_y$  and periodic boundary conditions. The  $z$  coordinates of all particles are non-negative and we choose the system size in the  $z$  direction to be much larger than the length of the chain.

### III. THE GROUND STATE

For the ground-state analysis we assume uniform tilt and head groups fixed to a triangular lattice with lattice constant  $a$ . Because we are interested in the case where  $c_{bl}, c_{ba} \gg \epsilon$  the bond angle and bond length potentials are idealized to be infinitely rigid for purposes of the ground-state analysis. This eliminates the corresponding degrees of freedom and thus simplifies the analysis considerably. In the following we present two types of calculations for the ground-state phase diagram:

- (i) a simple geometrical argument,
- (ii) energy minimization on the total potential energy surface.

Representing the Lennard-Jones force centers by hard spheres and assuming uniform tilt allows to view the system as a stack of planes of effective monomers. For  $a=d_0=1$  the spheres form a face centered cubic structure. In this case the tilt angle between the molecular axis and the surface normal is  $\arcsin(1/\sqrt{3})$ . By virtue of periodicity within the stack it is sufficient to look at only two of these planes. The spheres in the second plane form tetrahedrons within their adjacent spheres in the first plane and the tilt is directed into the next nearest neighbor chain direction (NNN direction). Decreasing the bond length  $d_0$  pulls the spheres in the second plane closer to one of their neighbors in the first plane while the distance to their other two neighbors in the first plane is kept constant at 1. This observation leads to a simple expression for the tilt angle  $\theta$  as a function of  $a$  and  $d_0$

$$\sin(\theta) = \frac{a^2 + d_0^2 - 1}{\sqrt{3}ad_0} \quad (4)$$

independent of chain length. The phase boundary between the tilted ( $\sin \theta > 0$ ) and the untilted ( $\sin \theta < 0$ ) phase is given by the condition  $a^2 + d_0^2 = 1$  describing a circle in the  $(a, d_0)$  plane.

In the second calculation the potential energy of one rod interacting with its uniformly tilted neighbors is minimized. The minimization is performed with respect to the tilt angle  $\theta$  and the tilt direction. The head separation  $a$  and bond length  $d_0$  are varied as parameters. The results of these calculations for different values of  $a$ ,  $d_0$  are summarized in Fig. 2 which shows the  $T=0$  phase boundary separating the tilted phase from the nontilted one. The data points shown in Fig.

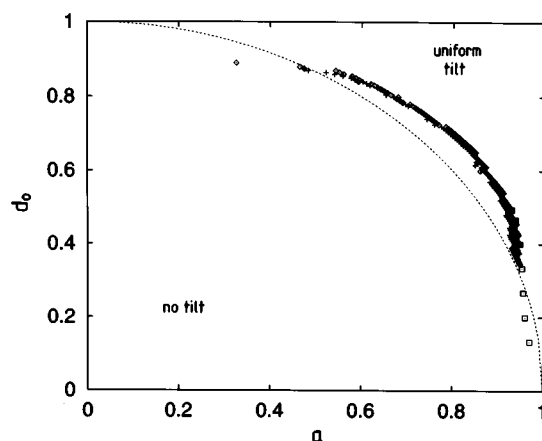


FIG. 2. The ground-state phase diagram in the  $(a, d_0)$  plane is plotted as calculated from the simple geometrical argument (line) and for the energy minimization for a LJ potential with cutoff at  $2\sigma$  (diamonds) and  $3\sigma$  (crosses). Squares represent data obtained in Ref. 11 for rods with 15 potential centers. The no-tilt phase at high densities is enclosed by the curves.

2 correspond to the points where the tilt angle drops to zero for the first time with decreasing  $a$  and fixed  $d_0$ . We invariably obtained next nearest neighbor tilt. The phase boundary is only slightly affected by the Lennard-Jones cutoff  $d_{LJ}$ . The boundary calculated from the hard sphere argument differs from that of the energy minimization because the geometrical argument applies only for hard core or very short ranged potentials. Systematic differences in the transition region, where the spheres in more than one tetrahedron become important are to be expected. For comparison we have also included in Fig. 2 the phase boundary from the ground-state analysis of the rigid rod model in Ref. 11. The dotted square data points are taken from Fig. 2 of Ref. 11 and they correspond to parameter values  $l=15$ ,  $c_{bl}=\infty$ , and  $c_{ba}=\infty$  in the present notation. The tilt angle as a function of  $a$  obtained

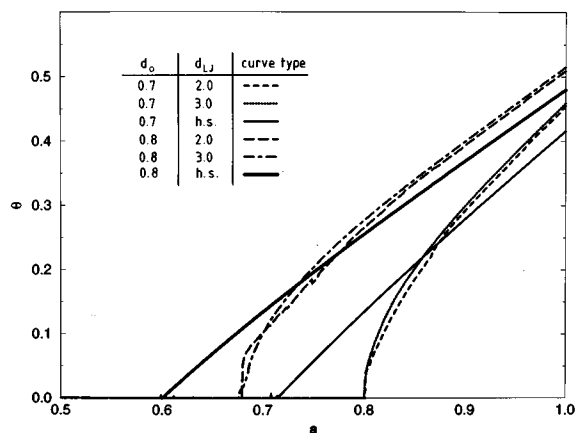


FIG. 3. The tilt angle at the ground state is plotted as a function of head lattice constant  $a$  for two different distances  $d_0$  of monomers along a chain (0.7 and 0.8) as calculated from energy minimization for LJ potentials with cutoff at  $2\sigma$  and  $3\sigma$ . The result of the "hard sphere" argument is also shown (denoted as h.s.).

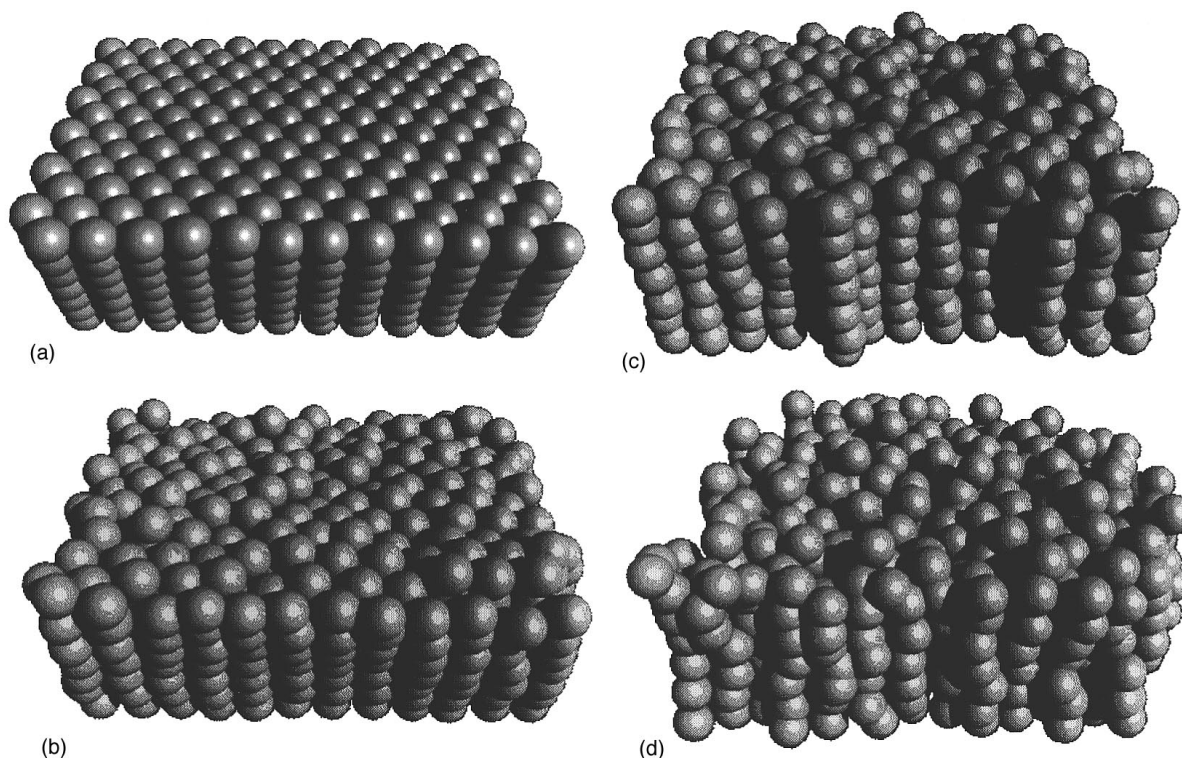


FIG. 4. Snapshot pictures at temperatures (a)  $T=0.1$ , (b)  $T=1.0$ , (c)  $T=2.0$ , (d)  $T=8.0$  for the system containing 144 chains. Each monomer is represented by a sphere of radius  $\sigma/2=0.5$ .

from (i) and (ii) is shown in Fig. 3 for two values of  $d_0$ . The results from (i) are in good qualitative agreement with our results for the Lennard-Jones potential for  $a \approx 1$  but fail again in the transition region.

#### IV. SIMULATIONAL DETAILS

To simulate the model at finite temperatures we employ a Metropolis Monte Carlo algorithm. A single monomer is randomly selected in each trial move. The maximum jump width is adjusted to optimize the acceptance rate and to prevent crossing of chain bonds. The restriction on the interaction range allows to employ a link-cell algorithm for storing the interacting neighbors.

We divide our simulation box into rectangular subcells of sidelength greater than or equal to this interaction length. In this way a particle in one subcell interacts only with particles in its own and adjacent cells. A special data structure is implemented to keep track of the cell contents. The data structure consists of linked lists of pointers onto a self-referencing vector starting from each cell. In this way the structures can be used recursively to take all cell members into consideration. The algorithm was tested extensively on dense polymer systems with and without obstacles.<sup>19</sup> The dimensions of the simulation box are chosen to fit a hexagonal monolayer structure, i.e.,  $L_x/L_y=2/\sqrt{3}$ . The density was taken to be  $2/\sqrt{3}$  chains per unit area corresponding to  $a=1$  for the lattice constant of the hexagonal lattice of head segments. The numbers of particles were chosen to support a

configuration with an even number of rows and columns. In the following we refer to the system sizes  $L_x=8$  and  $L_x=12$  mainly. At this density the spreading pressure is positive for the temperature range of interest, i.e., near the order-disorder transition. It was found however, that for low temperatures,  $T \rightarrow 0$ , negative spreading pressures occur. This is less serious than it may appear at first, because the uniformly tilted structure is still metastable under these conditions. At higher densities where the spreading pressure remains positive for  $T \rightarrow 0$  the pressure would become unphysically high at elevated temperatures. Such problems can be avoided by carrying out simulations in a constant spreading pressure ensemble. Because these are technically more demanding they have not been attempted here.

Scans over a broad temperature range were performed covering two decades in temperature ( $0.1 \leq T \leq 10$ ). For each temperature the first 20 000 Monte Carlo steps per monomer (MCS) were used for equilibration followed by 50 000 MCS for taking averages. Every 500th MCS was included in the average to suppress correlations between subsequent configurations. The simulations were carried out using several 100 hours of IBM RS 6000 370 CPU time.

To check for hysteresis in the measured quantities, we performed both heating and cooling runs. The heating runs were started from the ground-state configuration obtained by energy minimization at the lowest temperature. The results for small system sizes depend upon the box geometry. In the following we refer to the hexagonal box geometry introduced above where no significant hysteresis was observed.

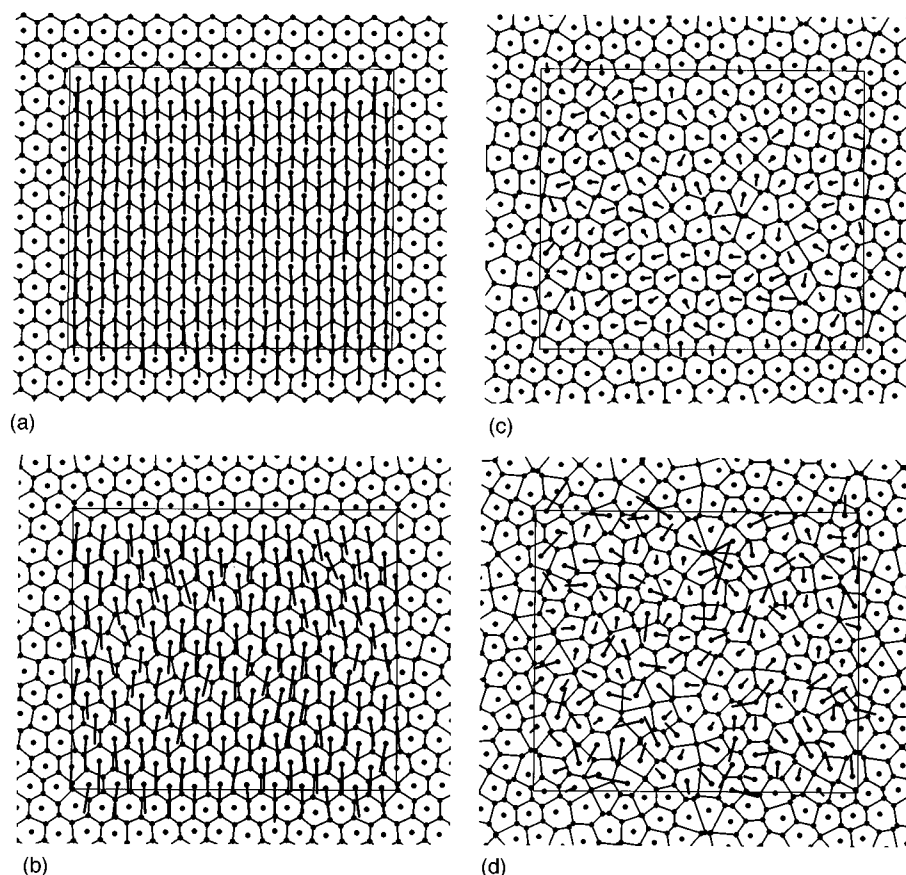


FIG. 5. Voronoi diagrams corresponding to the conformations in Fig. 4. (a)  $T=0.1$ , (b)  $T=1.0$ , (c)  $T=2.0$ , (d)  $T=8.0$ . The projection of the vector connecting the head group (denoted by a dot) and the end group of the surfactant molecule is shown together with the Voronoi tessellation for the head group lattice in the adsorption plane.

Additionally we considered a quadratic box as in Ref. 18 setting up 120 chains in an orthorhombically distorted conformation of ten rows and twelve columns inside a  $10 \times 10$  box. Large hysteresis loops are observed during heating and cooling runs, because a configuration with boundary induced defects and shear components of pressure in the adsorption plane is energetically preferable to a regular  $10 \times 12$  configuration.

## V. NUMERICAL RESULTS

### A. Configurations

Snapshots of the monolayer at different temperatures are shown in Fig. 4. At temperature  $T=0.1$  the configuration is in a crystalline state with uniformly tilted molecules. The chains are still in the tilted phase at  $T=1.0$  but with less orientational correlation and a lower tilt angle. At  $T=2.0$  the average tilt is almost zero.

In Fig. 5 the Voronoi constructions corresponding to the configurations in Fig. 4 are shown. The dots represent the lattice of head groups, the cells are the Voronoi cells. In addition the projections of the molecule directors into the  $xy$  plane are plotted. We choose the molecular directors  $\mathbf{D}$  to be the vectors connecting the end monomers of each chain. While at low temperatures the tilt is strictly towards next nearest neighbors no preferred tilt direction can be observed

by inspecting Fig. 5(b). At  $T=2.0$  the average tilt is rather small and defects begin to form in the head lattice.

### B. Density profiles

Figure 6 shows the monomer density profiles in the direction perpendicular to the substrate for each monomer at different temperatures. At low temperatures structures that consist of approximately equally spaced layers are formed. This justifies the assumption of the geometrical ground-state analysis. The distances between the topmost and bottommost layers to their neighboring layer is slightly higher than the other layer distances, because the end segments feel less Lennard-Jones interactions.

With increasing temperature the density distributions become broader. Because of the limited chain length, the uppermost monomers tend to fold back into lower layers at higher temperatures. This is indicated by the asymmetry of the monomer density distributions.

The total density profile in Fig. 7 shows that the layered structure is washed out with increasing temperature starting at the surface. During this surface melting process a film with uniform density is formed whose thickness increases with temperature. At the highest temperature  $T=8$  monomers from the second layer start to occupy defects in the head group lattice.

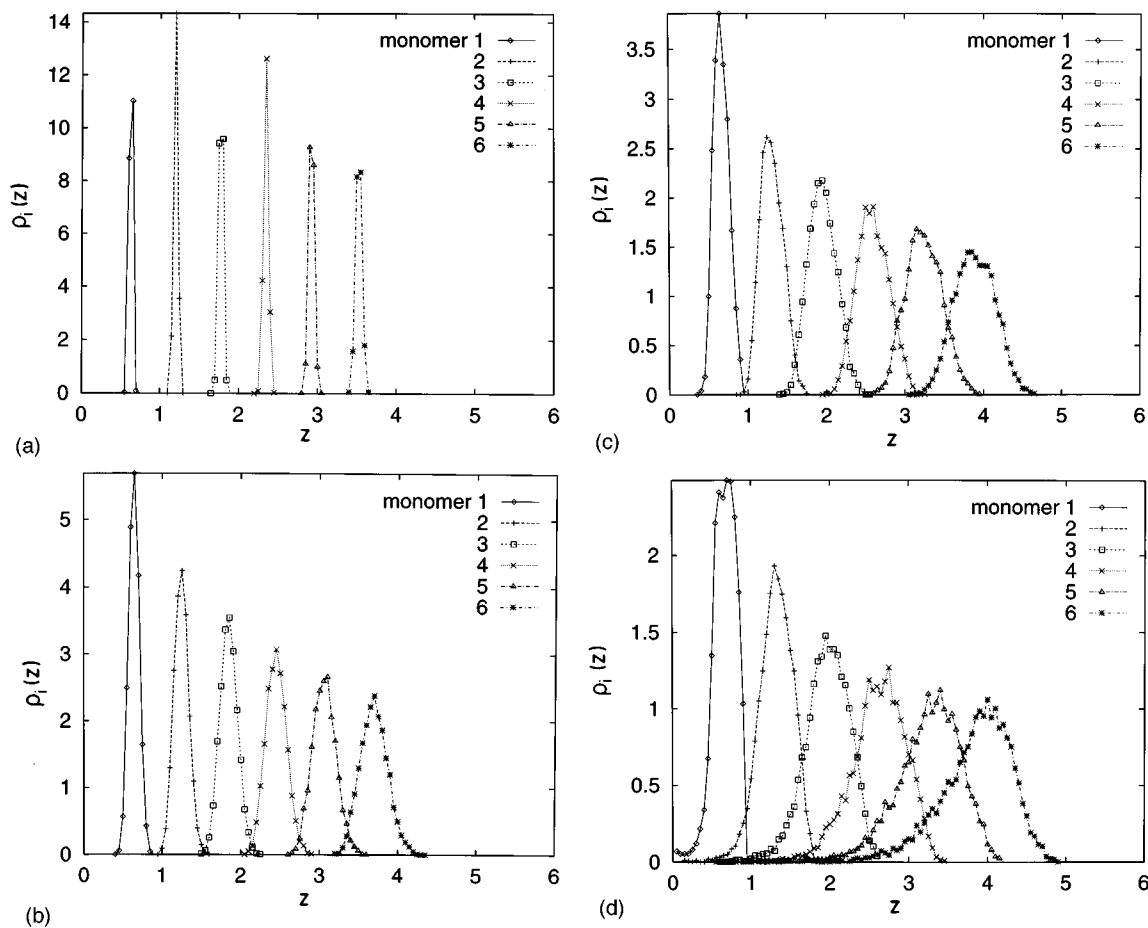


FIG. 6. Monomer density profiles  $\rho_i(z)$  in the  $z$  direction perpendicular to the grafting interface. Different curves belong to different monomers ( $i$ ) in a chain as indicated in the figure. (a)  $T=0.1$ , (b)  $T=1.0$ , (c)  $T=2.0$ , (d)  $T=8.0$ . All densities are normalized to one.

### C. Structure factor

We calculate two structure factors<sup>20</sup>

$$\frac{1}{n} \left| \sum_{j=1}^n e^{i(kr_j)} \right|^2 \quad (5)$$

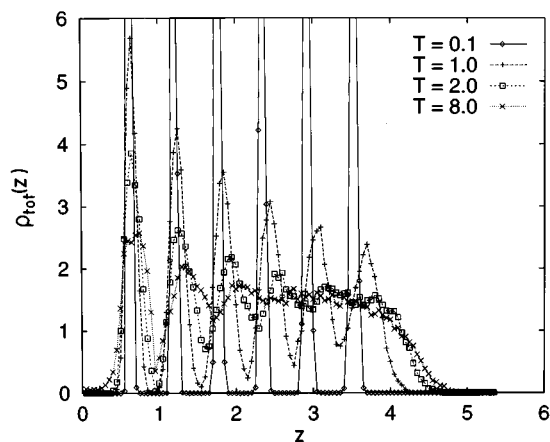


FIG. 7. Total monomer density profiles  $\rho_{\text{tot}}(z)$  in the  $z$  direction at temperatures as indicated in the figure. The densities are normalized to 6. Note that the grafted monomer at  $z=0$  (which would yield a  $\delta$  function there) is not included.

one for the head groups only denoted  $S_h(k)$  and one for all monomers denoted as  $S(k)$ . In the first case  $n$  is the number of head group monomers in the adsorption plane and  $r_j=(x_j, y_j)$  are their  $xy$  coordinates, in the second  $n$  denotes all monomers and  $r_j=(x_j, y_j)$  are the projections of their coordinates into the adsorption plane. Periodic boundary conditions imply that the components of the scattering vector  $k=(k_x, k_y)$  can only be multiples of  $2\pi/L_x$ ,  $2\pi/L_y$ .

The head group structure factor  $S_h(k)$  allows to study the positional order of the head lattice (see Fig. 8). Due to the relatively small system sizes under consideration we clearly cannot contribute to the discussion<sup>28</sup> about hexatic phases or quasi long range positional order in the low temperature phases. We observe a change from a hexagonal scattering pattern to a ring pattern at about  $T=8$  and therefore expect a second phase transition connected with the melting of the head group lattice to take place in this temperature regime.

The calculation of the structure factor for all monomers allows a better understanding of the monolayer structure as a whole. At low temperatures the film consists of hexagonal monomer layers packed one on top of each other, and displaced in NNN direction. For this reason the original hexagonal scattering pattern for one layer becomes modulated in the NNN direction in the overall structure factor in Fig. 9. As

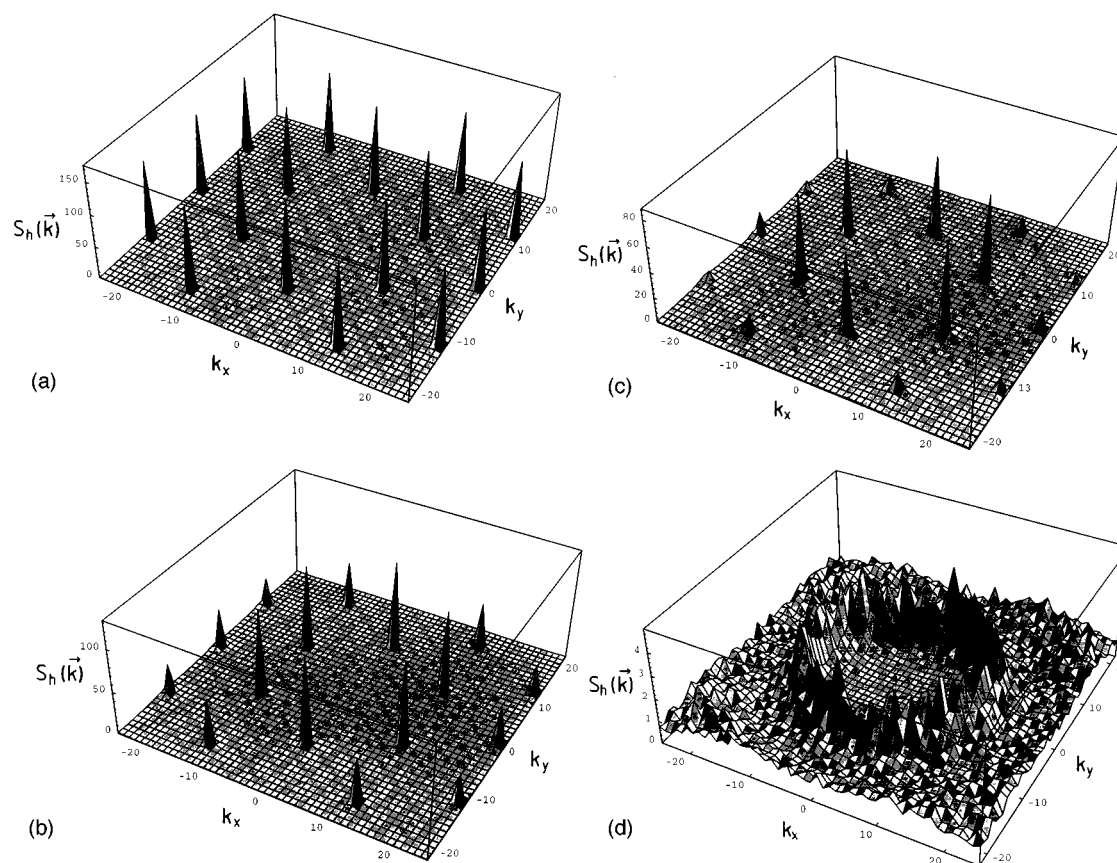


FIG. 8. Plot of the structure factor  $S_h(\mathbf{k})$  for head monomers ( $n=144$ ). (a)  $T=0.1$ , (b)  $T=1.0$ , (c)  $T=2.0$ , (d)  $T=8.0$ . The units of  $k_x$  are chosen as  $2\pi/L_x$  and the units of  $k_y$  as  $2\pi/L_y$ , respectively.

the positional correlation between different layers disappears with increasing temperature the hexagonal pattern reappears. The ring pattern is observed again at about  $T=8$ .

#### D. Tilt order

The average of the absolute value of the tilt angle defined as the angle between the molecular director and the surface normal is shown in Fig. 10 as a function of temperature. It decreases monotonically until  $T \approx 2$  and then increases again. This increase is caused by stronger tilt angle fluctuations in the chain configurations especially after the melting transition at  $T \approx 8$ . (Note that the average of the absolute value of the tilt angle in the disordered phase where the mean tilt angle is zero is proportional to the width of the (Gaussian) distribution of this angle which increases with temperature.) This is corroborated by the probability distributions for finding a molecule with a given projection of the molecular director  $\mathbf{D}$  into the  $xy$  plane shown in Fig. 11. At low temperatures the distribution is sharply peaked at  $\mathbf{D} \neq 0$ . The expectation value is shifted to zero during the tilting transition while the distribution becomes broader.

#### E. NN bond orientational correlation in the head lattice

Thin films are intermediate between two- and three-dimensional systems. Our monolayer model system can be viewed as a two-dimensional system of head monomers with

internal degrees of freedom. It is therefore interesting to investigate how the two-dimensional melting process of the head monomers in the adsorption plane is affected by the behavior of the chains connected to them, respectively, how the restoration of ergodicity propagates through the adsorption plane.

For this purpose we study the absolute value of the following quantity:

$$\Psi_6 = \frac{1}{n} \sum_{i=1}^n \frac{1}{6} \sum_{j=1}^6 e^{i6\theta_{ij}}, \quad (6)$$

where  $\theta_{ij}$  is the angle between the line connecting head monomer  $i$  with its nearest neighbor  $j$  and a reference axis. The actual choice of the reference axis will only result in a constant phase within the absolute value and therefore will not affect the overall result. Since it is too time consuming to perform a Voronoi construction each time of measurement, we always sum over the six neighbors with lowest distance. For a review about bond-orientational order see, for example, Refs. 29 and 30.

The correlation  $\Psi_6$  function starts at unity at low temperatures (Fig. 12). A change in slope occurs at about  $T=2$  near the expected tilt transition indicating that head-lattice order is coupled to the orientational order of the chains. The strong further decrease near  $T=8$  and the onset of strong size effects are further indications of the melting transition.

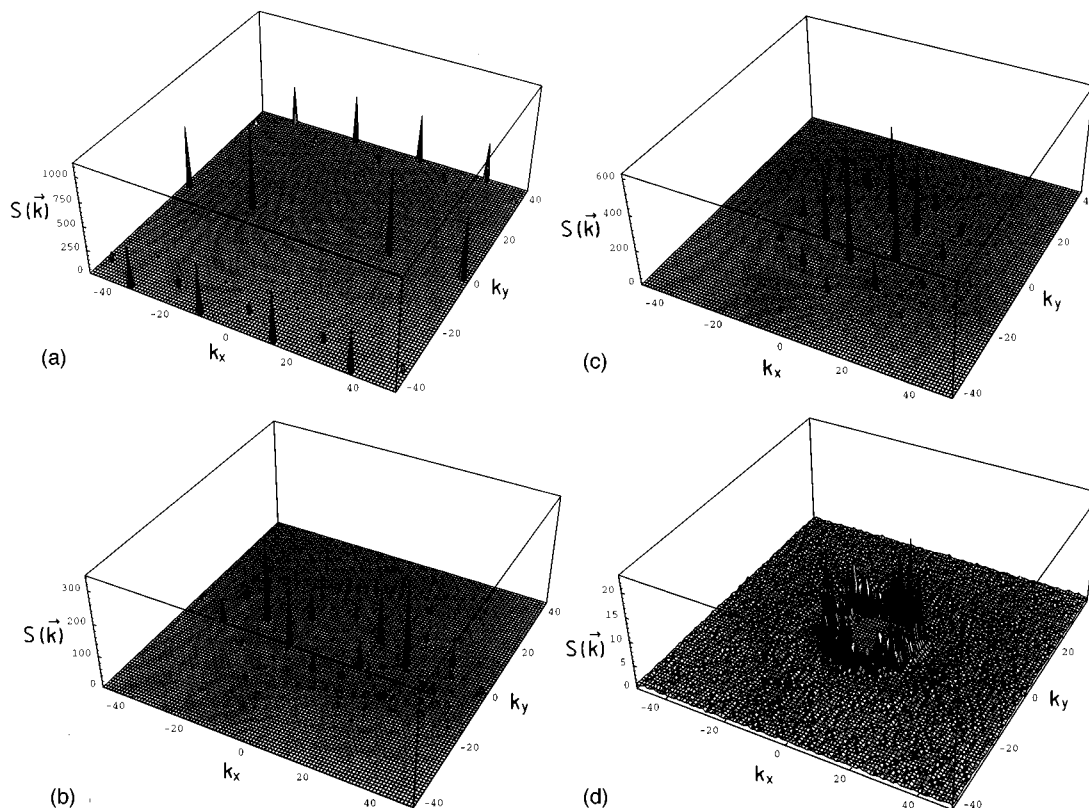


FIG. 9. The 2-D structure factor  $S(\mathbf{k})$  for all monomers ( $n=7 \times 144$ ). (a)  $T=0.1$ , (b)  $T=1.0$ , (c)  $T=2.0$ , (d)  $T=8.0$ . The units of  $k_x$  are chosen as  $2\pi/L_x$  and the units of  $k_y$  as  $2\pi/L_y$ , respectively.

### F. Orientational correlation of bonds within a chain

A bond order parameter for each bond,  $i$ , along a chain can be calculated from

$$S_i = \frac{1}{2} \langle [3 \cos^2(\Theta_i) - 1] \rangle, \quad (7)$$

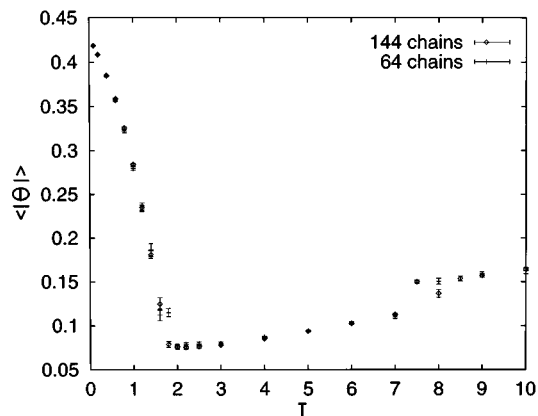


FIG. 10. Average tilt angle as a function of temperature. The tilt angle  $\theta$  is defined as the angle between the vector connecting head and end group of a molecule and the  $z$  axis. The symbols belong to the system sizes indicated in the figure.

where  $\Theta_i$  is the angle formed by the bond vector connecting the  $i$ th and  $(i+1)$ th chain segment and the molecular director (see Fig. 1). The correlation functions are shown in Fig. 13;  $S_i$  decrease monotonically with temperature. The changes in slope at  $T=2$  and  $8$  indicate the phase transitions.  $S_1$  and  $S_6$  fall off most strongly because the end segments of each chain feel only one chain neighbor. The distribution of the bond angles  $\theta_i$  is not expected to yield significant structural information about different phases,<sup>31</sup> and thus is not reproduced here.

### G. Orientational correlations between nearest neighbor (NN) chains

The quantity

$$K_{\text{NN}} = \left\langle \frac{1}{6} \sum_{\text{NN}} \frac{1}{2} [3 \cos^2(\theta_{\text{NN}}) - 1] \right\rangle \quad (8)$$

measures the orientational correlations between NN chains.  $\theta_{\text{NN}}$  is the relative angle between two NN chains. As above the nearest neighbor chains are always taken to be six chains with lowest head segment distance to the initial chain head group.

For steric reasons this quantity gives a rather high value ( $0.88 < K_{\text{NN}} < 1$ ) for all considered temperatures (Fig. 14).

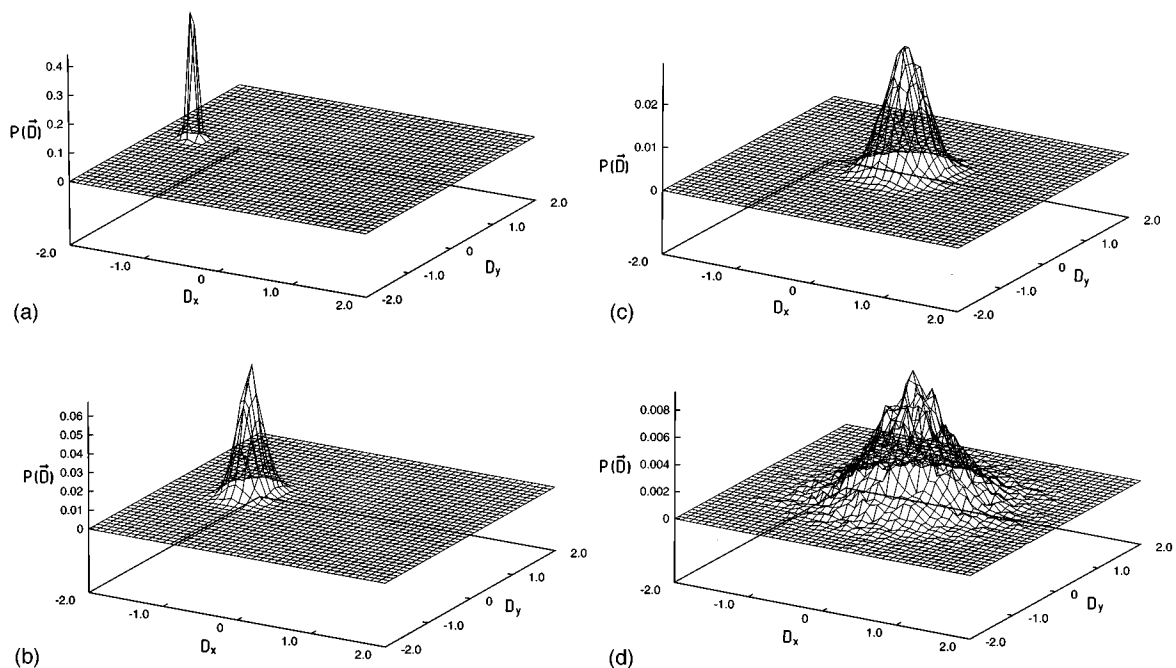


FIG. 11. Probability of projections  $P(\mathbf{D})$  of molecular directors  $\mathbf{D}=(D_x, D_y)$  into the adsorption plane for temperatures (a)  $T=0.1$ , (b)  $T=1.0$ , (c)  $T=2.0$ , (d)  $T=8.0$ .

The sharp decrease of  $K_{NN}$  at about  $T=8$  is a further corroboration of the melting transition in this temperature region.

## VI. DISCUSSION

In the present model we have studied a coarse-grained model for lipid monolayers or dense layers of alkane-type surfactants endgrafted at surfaces using an off-lattice Monte Carlo technique. The surfactant molecules were represented by chains consisting of seven effective monomers, the first of which (the head group) was fixed in the plane  $z=0$ . This

model was designed to study phase transitions in the high density regime, where lattice models are problematic. At densities corresponding to a uniformly tilted ground state, we find at least two distinct temperature driven phase transitions on the basis of our data. The transformation at lower temperatures is characterized by a continuous decrease in tilt angle. The low temperature phase resembles a bulk crystalline phase while at higher temperatures, as may be inferred from Figs. 6(c), 7(c), and 8(c), the fluidized tail groups coexist with frozen crystalline head groups. This situation corresponds to a highly constrained surface melting transition. A second phase transition at much higher temperatures is ap-

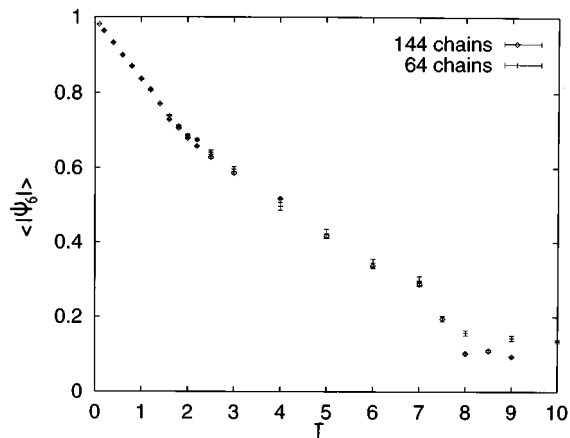


FIG. 12. NN bond orientational correlation function  $\langle |\Psi_6| \rangle$  as a function of temperature.

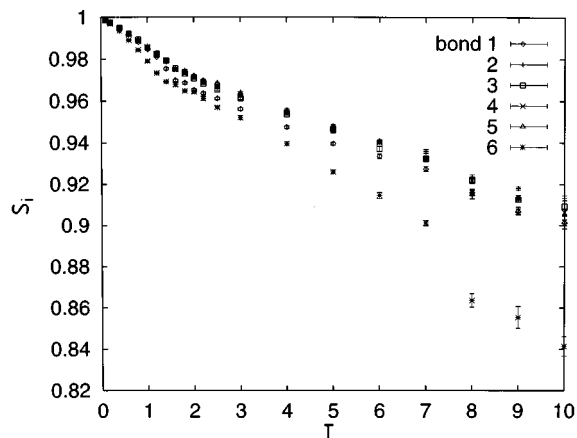


FIG. 13. Bond order parameter  $S_i$  for bond number  $i=1, \dots, 6$  as a function of temperature.

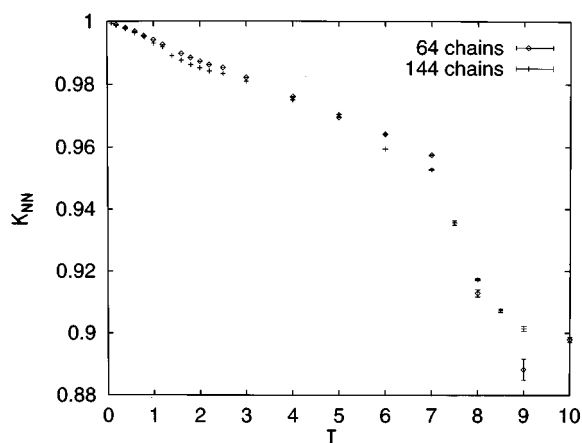


FIG. 14. Orientational correlation function  $K_{NN}$  as a function of temperature.

parent from our data. In that transition also the previously frozen head group lattice melts, and the coexistence of a quasi-ergodic surface of tail groups and a quasi-nonergodic surface of head groups disappears into a surface grafted polymer melt.

The phase diagram of our model certainly is still much simpler than the phase diagram expected for Langmuir monolayers. This simplicity is presumably due to several oversimplifications in our model which are driven by the need for computational feasibility. Among these are the inadequate modeling of the head groups and the head group-surface interactions. Due to our overidealizations the solid phase of our system exhibits a simple stacking of planes with a close-packed triangular lattice, while in solid alkanes one has a stacking of planes with a herringbone-type orientational order. It would be interesting to develop a coarse-grained model where this additional local order parameter is present.<sup>32</sup>

## ACKNOWLEDGMENTS

We are grateful to H. Möhwald and I. R. Peterson for stimulating discussions. One of us (F. M. H.) received partial support from the Graduiertenkolleg "Physik und Chemie su-

pramolekularer Systeme" der Deutschen Forschungsgemeinschaft, and one of us (R. H.) acknowledges the Commission of the European Communities (ERBCHBGCT920180) for financial support.

- <sup>1</sup>C. M. Knobler and R. C. Desai, *Ann. Rev. Phys. Chem.* **43**, 207 (1992).
- <sup>2</sup>A. M. Bibo, C. M. Knobler, and I. R. Peterson, *J. Chem. Phys.* **95**, 5591 (1991).
- <sup>3</sup>D. Andelman, F. Brochard, C. M. Knobler, and F. Rondelez, in *Micelles, Membranes, Microemulsions, and Monolayers*, edited by M. Gelbart, A. Ben Shaul, and D. Roux (Springer, New York, 1994), pp. 559–602.
- <sup>4</sup>H. Möhwald, *Ann. Rev. Phys. Chem.* **41**, 441 (1990).
- <sup>5</sup>J. Hautman and M. L. Klein, *J. Chem. Phys.* **93**, 7483 (1990).
- <sup>6</sup>J. B. Bareman and M. L. Klein, *J. Phys. Chem.* **94**, 5202 (1990).
- <sup>7</sup>J. Hautman, J. B. Bareman, W. Mar, and M. L. Klein, *J. Chem. Soc. Faraday Trans.* **87**, 2031 (1991).
- <sup>8</sup>M. Milik, A. Kolinski, and J. Skolnick, *J. Chem. Phys.* **93**, 6 (1990).
- <sup>9</sup>H. Stettin, J. H. Mögel, and R. Friedemann, *Ber. Bunsenges. Phys. Chem.* **7**, 44 (1993).
- <sup>10</sup>F. M. Haas, P.-Y. Lai, and K. Binder, *Makromol. Chem., Theory Simul.* **2**, 889 (1993).
- <sup>11</sup>M. Kreer, K. Kremer, and K. Binder, *J. Chem. Phys.* **92**, 6195 (1990).
- <sup>12</sup>M. Scheringer, R. Hilfer, and K. Binder, *J. Chem. Phys.* **96**, 2269 (1992).
- <sup>13</sup>J. Harris and S. A. Rice, *J. Chem. Phys.* **89**, 5898 (1988).
- <sup>14</sup>G. Cardini, P. Bareman, and M. L. Klein, *Chem. Phys. Lett.* **145**, 493 (1988).
- <sup>15</sup>J. Hautman and M. L. Klein, *J. Chem. Phys.* **91**, 4994 (1989).
- <sup>16</sup>M. Bishop and J. H. Clarke, *J. Chem. Phys.* **95**, 540 (1991).
- <sup>17</sup>M. A. Moller, D. J. Tildesley, and K. S. Kim, *J. Chem. Phys.* **94**, 8390 (1991).
- <sup>18</sup>S. A. Safran, M. O. Robbins, and S. Garoff, *Phys. Rev. A* **33**, 2186 (1986).
- <sup>19</sup>R. Hilfer (unpublished).
- <sup>20</sup>S. Karaborni and S. Toxvaerd, *J. Chem. Phys.* **96**, 5505 (1992); **96**, 4965 (1992).
- <sup>21</sup>A. Ulman, *An Introduction to Ultrathin Organic Films* (Academic, San Diego, 1991).
- <sup>22</sup>G. Hoehner, M. Kinzler, Ch. Wöll, M. Grunze, M. K. Scheller, and L. S. Cederbaum, *Phys. Rev. Lett.* **67**, 851 (1991).
- <sup>23</sup>D. A. Outka, J. Stöhr, J. P. Rabe, and J. D. Swalen, *J. Chem. Phys.* **88**, 4076 (1988).
- <sup>24</sup>M. Kinzler, A. Schertel, G. Höhner, Ch. Wöll, M. Grunze, H. Albrecht, G. Holzhiuter, and Th. Gerber, *J. Chem. Phys.* **100**, 7722 (1994).
- <sup>25</sup>CS. Gau, H. Yu, and G. Zograf, *Macromolecules* **26**, 2524 (1993).
- <sup>26</sup>J. Baschnagel, K. Qin, W. Paul, and K. Binder, *Macromolecules* **25**, 3117 (1992).
- <sup>27</sup>J. Baschnagel, K. Binder, W. Paul, M. Laso, U. Suter, I. Batoulis, W. Jilge, and T. Bürger, *J. Chem. Phys.* **95**, 6014 (1991).
- <sup>28</sup>D. R. Nelson and B. I. Halperin, *Phys. Rev. B* **21**, 21 (1989).
- <sup>29</sup>K. J. Strandburg, *Rev. Mod. Phys.* **60**, 161 (1988).
- <sup>30</sup>K. J. Strandburg, *Bond-Orientational Order in Condensed Matter Systems* (Springer, Berlin, 1992).
- <sup>31</sup>R. Hilfer, F. M. Haas, and K. Binder: *Nuovo Cimento* (in press, 1994).
- <sup>32</sup>V. M. Kaganer and E. B. Loginov, *Phys. Rev. Lett.* **71**, 2599 (1993).